

# Primordial Black Hole Formation from the Upward Step Model: Avoiding Overproduction

Xiaoding Wang,<sup>a</sup> Xiao-Han Ma,<sup>b,c,d,e</sup> Yi-Fu Cai<sup>b,c,d</sup>

<sup>a</sup>The Key Laboratory of Cosmic Rays (Tibet University), Ministry of Education, Lhasa 850000, Tibet, China

<sup>b</sup>Department of Astronomy, School of Physical Sciences, University of Science and Technology of China, Hefei, Anhui 230026, China

<sup>c</sup>CAS Key Laboratory for Research in Galaxies and Cosmology, School of Astronomy and Space Science, University of Science and Technology of China, Hefei, Anhui 230026, China

<sup>d</sup>Deep Space Exploration Laboratory, Hefei 230088, China

<sup>e</sup>Kavli Institute for the Physics and Mathematics of the Universe (WPI), UTIAS The University of Tokyo, Kashiwa, Chiba 277-8583, Japan

E-mail: [mxh171554@mail.ustc.edu.cn](mailto:mxh171554@mail.ustc.edu.cn)

**Abstract.** We investigate the formation of primordial black holes (PBHs) in an upward step inflationary model, where nonlinearities between curvature perturbations and field fluctuations introduce a cutoff, deviating from the Gaussian case. This necessitates a reevaluation of PBH formation, as  $\mathcal{R}$  is not the optimal variable for estimating abundance. Using the extended Press-Schechter formalism, we show that non-Gaussianity modifies both the curvature perturbation profile  $\mathcal{R}(r)$  and the integration path in probability space, significantly impacting PBH abundance. Our results reveal that the abundance initially increases with the parameter  $h$ , which characterizes the relaxation stage after the step. However, beyond a critical value ( $h \simeq 5.9$ ), it sharply declines before rising again. Furthermore, we demonstrate that non-Gaussianity introduces uncertainties in indirect PBH observations via gravitational waves. Notably, we present an example where a positive  $f_{\text{NL}}$  does not necessarily enhance PBH production, contrary to conventional expectations. Finally, by accounting for non-perturbative effects, we resolve the overproduction of PBHs suggested by pulsar timing array (PTA) data, underscoring the critical importance of incorporating non-Gaussianity in future studies.

---

## Contents

<b>1</b>	<b>Introduction</b>	<b>1</b>
<b>2</b>	<b>Revisiting upward step model</b>	<b>3</b>
<b>3</b>	<b>PBH formation in upward step model</b>	<b>6</b>
3.1	Basic setup for extended Press-Shecheter formalism	6
3.2	PBH abundance	9
<b>4</b>	<b>Implications for indirect observations of PBHs</b>	<b>14</b>
4.1	Energy density spectrum of SIGWs	14
<b>5</b>	<b>Conclusion</b>	<b>15</b>

---

## 1 Introduction

PBHs have become one of the most compelling topics, captivating the attention of cosmologists and astrophysicists for over a decade, as their existence offers a natural explanation for numerous mysteries in modern cosmology. Unlike black holes formed from stellar collapse, PBHs originate in the primordial universe and result from the collapse of disturbed primordial radiation fields [1–3]. They decoupled from baryons in the very early universe and thus can be considered candidates for dark matter [4]. Furthermore, PBHs of various masses can seed the formation of supermassive black holes (SMBHs) observed by the James Webb Space Telescope (JWST) in the early universe [5], directly or indirectly source the gravitational waves detected by LIGO/VIRGO [6–10], and PTAs collaborations (NANOGrav [11, 12], EPTA [13–15], PPTA [16–18] and CPTA [19]) and even heat our universe through Hawking radiation before big bang nucleosynthesis (BBN) [20]. This capability is due to the fact that the mass of PBHs depends both on the size of the Hubble horizon at the time of their formation and on primordial fluctuations. Consequently, PBHs are able to surpass the mass limits typically associated with astrophysically formed black holes.

Since PBHs form from the collapse of the overdense regions in the very early universe, the statistics of primordial fluctuations and the criteria for collapse determine both their initial abundance and initial mass function. These are crucial properties that allow us to search for PBHs. On the other hand, detecting PBHs also serves as a smoking gun, providing insights into the physics behind primordial fluctuations and revealing the unknown history of the early universe.

From the latest cosmic microwave background (CMB) observations, we know that the comoving curvature perturbation  $\mathcal{R}$  is nearly scale invariant, quasi-adiabatic and Gaussian on large scale [21]. Specifically,  $\mathcal{P}_{\mathcal{R}}(k) = A_s(k/k_{\text{pivot}})^{n_s-1}$  with  $A_s \simeq 2 \times 10^{-9}$ ,  $n_s \simeq 0.96$  and  $k_{\text{pivot}} = 0.05 \text{ Mpc}^{-1}$ . If perturbations at smaller scales exhibit the same characteristics, the chances of PBHs formation in our universe are minimal. However, various indications suggest that the power spectrum of curvature perturbations was enhanced at smaller scales, leading to a rich set of phenomenological effects, including the formation of detectable PBHs and the generation of scalar-induced gravitational waves (SIGWs).

The observation of a stochastic gravitational wave background in the nHz band by PTAs in 2023 appears to suggest that these signals may originate from an enhanced primordial power spectrum, with  $\mathcal{P}_{\mathcal{R}} \sim 10^{-1}$  [22–24]. Subsequently, it was realized that if all gravitational wave signals were induced by enhanced scalar perturbations, PBHs produced simultaneously should also have been observed, yet they remain undetected in current direct observations. This results in the PBH overproduction problem, which may suggest the non-Gaussianity of primordial perturbations.

Instead of using the curvature perturbation on comoving slices  $\mathcal{R}$  or the density contrast  $\delta\rho/\rho$ , the compaction function  $\mathcal{C}(r, t, \mathbf{x}) \equiv 2\delta M(r, t, \mathbf{x})/L(r, t)$ , where  $L(r, t)$  is the areal radius, is now commonly employed as the appropriate variable for calculating the abundance of PBHs [24–30]. Following the same philosophy as the Press-Schechter formalism used to calculate the halo mass function, the extended Press-Schechter formalism calculates the abundance of PBHs by integrating the probability density function (PDF)  $\mathbb{P}(\mathcal{C})$  from the threshold. In the Gaussian scenario, all necessary information for the PDF is encapsulated within the power spectrum  $\mathcal{P}_{\mathcal{R}}$ . This dependency is critical for constraining PBHs through indirect observations, including SIGWs.

When non-Gaussianity is taken into account, describing it becomes crucial. Researchers use non-Gaussianity parameters to discuss local non-Gaussianity, such as  $f_{\text{NL}}$  and  $g_{\text{NL}}$ , based on a perturbative series of the random variable:

$$\mathcal{R}(\mathbf{x}) = \mathcal{R}_{\text{G}}(\mathbf{x}) + \frac{3}{5}f_{\text{NL}} [\mathcal{R}_{\text{G}}^2(\mathbf{x}) - \langle \mathcal{R}_{\text{G}}^2(\mathbf{x}) \rangle] + g_{\text{NL}}\mathcal{R}_{\text{G}}^3(\mathbf{x}) + \dots, \quad (1.1)$$

where  $\mathcal{R}_{\text{G}}(\mathbf{x})$  denotes the Gaussian random field. This expression provides a model-independent description of local non-Gaussianity and is widely adopted in the literature. Using this perturbative but model-independent approach, several studies have revealed the non-Gaussian effects on SIGWs and PBHs [24, 31–35]. However, this perturbative approach may not be effective when there is a significant non-Gaussian tail. Specifically, when calculating the abundance of PBHs, we are analyzing statistics related to rare events described by the tail of the PDF. Recently, several works have investigated the formation of PBHs in the presence of a non-Gaussian tail [36–41]. Analysis of the latest 15-year dataset released by PTAs in 2023 indicated that non-Gaussian primordial perturbations with a positive  $f_{\text{NL}}$  tend to exacerbate the PBH overproduction problem [24, 32, 42–46], leading to the disfavoring of several models, including those with an upward step feature in the inflaton potential [47].

However, a positive  $f_{\text{NL}}$  does not always enhance the abundance of PBHs when non-perturbative features play a role in the tail of the PDF. In models with an upward step in the inflaton potential, there exists a cutoff in the PDF of curvature perturbations [41], which can significantly boost or suppress the PBH abundance. In this work, we demonstrate that upward step models can still potentially produce the stochastic gravitational wave background (SGWB) observed by PTAs without the overproduction of PBHs, even when  $f_{\text{NL}}$  is positive, by employing the extended Press-Schechter formalism. This simple example shows how the abundance of PBHs can deviate greatly from calculations based on the primordial scalar power spectrum with corrections from  $f_{\text{NL}}$ .

The paper is organized as follows: In Section 2, we revisit the single-field inflation model with an upward step in the inflaton potential and analyze the non-Gaussian tail of the curvature perturbation using the  $\delta N$  formalism. In Section 3, we set up the extended Press-Schechter formalism and estimate PBH formation in the slow-roll-step-slow-roll model. In Section 4, we discuss the SIGWs accompanying PBH formation and reconsider the issue

of overproduction by accounting for non-perturbative non-Gaussianity. Section 5 is devoted to the conclusion.

## 2 Revisiting upward step model

In a standard single-field inflation scenario, the slow-roll (SR) phase is necessary to produce a nearly scale-invariant power spectrum  $\mathcal{P}_{\mathcal{R}_G}$  at CMB scales. The slow-roll conditions are:

$$\varepsilon_H \equiv -\frac{\dot{H}}{H^2} \ll 1, \quad |\eta_H| \equiv \left| \frac{\dot{\varepsilon}_H}{H\varepsilon_H} \right| \ll 1, \quad (2.1)$$

which ensure that inflationary expansion lasts long enough. In models with a canonical kinetic term,  $K \propto \partial_\mu \phi \partial^\mu \phi$ , the slow-roll condition is typically interpreted as the requirement for a sufficiently flat potential  $V(\phi)$ . We use ‘ $\cdot$ ’ denotes the derivative with respect to comoving cosmic time  $t$ . However, PBH formation often demands non-trivial features in  $V(\phi)$ , such as an inflection point or step-like features [41, 48–62]. These non-trivial features cause the inflaton to deviate from the slow-roll phase, thereby enhancing the scalar power spectrum and generating non-Gaussianity on specific scales. To discuss the non-perturbative non-Gaussianity (i.e., the non-Gaussian tail) in the upward step model and its application to PBH formation in light of 15-year PTAs observations, we revisit the upward step model here. We consider a piecewise potential joined by an upward step, with a height  $\Delta V$ , parameterized as follows,

$$V(\phi) = V_0 [1 + \sqrt{2\varepsilon_I} (\phi - \phi_*)] \Theta(\phi - \phi_*) + (V_0 + \Delta V) [1 + \sqrt{2\varepsilon_{II}} (\phi - \phi_*)] \Theta(\phi_* - \phi), \quad (2.2)$$

where  $\Theta(x)$  is the Heaviside step function<sup>1</sup>.

The Friedmann equations and the equation of motion for the inflaton  $\phi$  in the flat Friedmann-Lemaître-Robertson-Walker (FLRW) background are expressed as

$$3M_{\text{pl}}^2 H^2 = \frac{1}{2} \dot{\phi}^2 + V(\phi), \quad (2.3)$$

$$M_{\text{pl}}^2 \dot{H} = -\frac{1}{2} \dot{\phi}^2, \quad (2.4)$$

$$\ddot{\phi} + 3H\dot{\phi} + V_{,\phi} = 0. \quad (2.5)$$

For simplicity, we use the convention that the reduced Planck mass  $M_{\text{pl}} \equiv \sqrt{1/8\pi G} = 1$  to simplify the expressions. Here,  $V_{,\phi}$  represents the derivative of  $V(\phi)$  with respect to  $\phi$ . It is more convenient to rewrite the Klein-Gordon (K-G) equation using the e-folding number  $dn = Hdt$  as a time variable:

$$\frac{d^2\phi}{dn^2} + (3 - \varepsilon_H) \frac{d\phi}{dn} + \frac{V_{,\phi}}{H^2} = 0. \quad (2.6)$$

In this model with a canonical kinetic term,  $\Delta V/V$  is usually small to ensure a healthy end to inflation (whereas for non-canonical cases, the inflaton can overcome much steeper barriers

---

<sup>1</sup>In a realistic model, we first reformulate the second part of (2.2) into  $V_0 + [\Delta V + (V_0 + \Delta V)\sqrt{\varepsilon_{II}}(\phi - \phi_*)]\Theta(\phi_* - \phi)$ , subsequently employing Hermitian interpolation to define a smoothed step function  $\Theta_s(x; \lambda)$ , which replaces the Heaviside step function  $\Theta(\phi_* - \phi)$ . The smoothed step function  $\Theta_s(x; \lambda)$  ensures the continuity of the first derivative of  $V(\phi)$ , where  $\Theta_s(x; \lambda) \equiv \lambda x + \lambda x(\lambda x - 1) [1 - 2\lambda x + (1 - \lambda x)V_0\sqrt{2\varepsilon_I}/(\lambda\Delta V)]$  for  $0 < \lambda x < 1$ . When  $\lambda x < 0$ ,  $\Theta_s(x; \lambda) = 0$ , and when  $\lambda x > 1$ ,  $\Theta_s(x; \lambda) = 1$ .

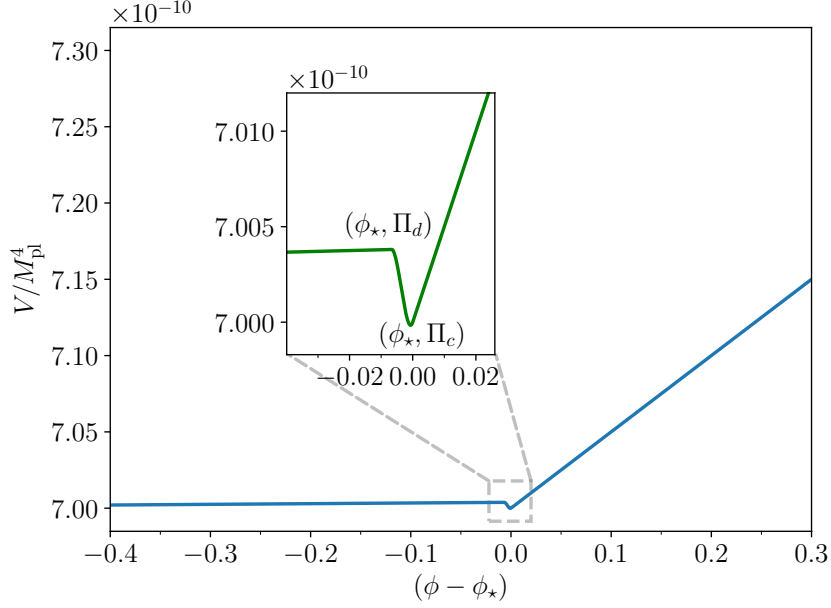


**Figure 1.** The inflationary potential  $V(\phi)$  is given by (2.2). The parameters are chosen as  $V_0 = 7 \times 10^{-10} M_{\text{pl}}^4$ ,  $\Delta V = 3.85805 \times 10^{-13} M_{\text{pl}}^4$ ,  $\epsilon_I = 2.551 \times 10^{-3}$ ,  $\epsilon_{II} = 4.077 \times 10^{-7}$ , and  $\lambda = 1.5 \times 10^2$ .

[63]). Thus, when examining the dynamics near the sharp upward step,  $H$  can be considered constant, leading to a nonlinear relationship between the field velocity before and after the step.

$$\Pi_d \simeq \sqrt{\Pi_c^2 - 6 \frac{\Delta V}{V}}, \quad (2.7)$$

where the inflaton's momentum is defined as  $\Pi \equiv -d\phi/dn$ .

Substitute the potential (2.2) into K-G equation and ignore the  $\epsilon_H$  term, then we have

$$\frac{d^2\phi}{dn^2} + 3 \frac{d\phi}{dn} + 3\sqrt{2\epsilon_X} = 0, \quad (2.8)$$

which gives the solution:

$$\phi(n) = C_{1,X} e^{-3(n-n_*)} - \sqrt{2\epsilon_X}(n - n_*) + C_{2,X}, \quad (2.9)$$

where the coefficients  $C_{1,X}$  and  $C_{2,X}$  are determined by matching condition at  $\phi_*$ . This solution suggests that the phase  $(\phi(n), \Pi(n))$  of the system can be expressed as:

$$3\phi(n) - \Pi(n) = -3\sqrt{2\epsilon_X}(n - n_*) + 3C_{2,X} - \sqrt{2\epsilon_X}. \quad (2.10)$$

The parameter  $\phi_*$ , which determines the location of the step, is set by the model. Thus, in the classical regime (ignoring the diffusion noise from sub-horizon fluctuations, i.e., quantum diffusion, see [64–66]), the dynamics of the second stage are fully governed by the phase at the top of the step  $(\phi_*, \Pi_d)$ . The sudden change in field velocity, as given by (2.7), can push the inflaton significantly away from the attractor solution, with the subsequent relaxation

leading to several non-trivial phenomena. Thus, it is convenient to define two dimensionless parameters here:

$$g \equiv \frac{\Pi_d}{\Pi_c}, \quad h \equiv \frac{6\sqrt{2\epsilon_{II}}}{\Pi_d}, \quad (2.11)$$

Here,  $0 < g < 1$  quantifies the velocity loss due to the upward step, and  $h > 0$  measures the deviation of the initial velocity  $\Pi_d$  from the slow-roll attractor in the second stage<sup>2</sup>.

The enhancement of the power spectrum of curvature perturbations was initially observed and later applied to generate PBHs. As discussed in [41], by solving the Sasaki-Mukhanov equation with appropriate matching conditions at the step, the power spectrum of curvature perturbations  $\mathcal{R}_{G,k}$  exiting the horizon near  $\phi_c$  is enhanced by a factor of  $g^{-2}$ , allowing it to easily meet the condition for producing PBHs as dark matter,  $\mathcal{P}_{\mathcal{R}_G} \simeq 10^{-2}$ .

In addition to the amplitude and location of the peak, the growth behavior before the peak, as well as the IR and UV behavior of  $\mathcal{P}_{\mathcal{R}_G}(k)$ , are discussed in detail. For clarity in the subsequent discussion, we summarize the key features of the power spectrum for the SR-upward-step-SR model here:

$$\mathcal{P}_{\mathcal{R}_G}(k) \simeq \begin{cases} \frac{1}{2\epsilon_I} \left(\frac{H}{2\pi}\right)^2; & \text{IR part,} \\ k^4; & k^4 \text{ growth before the peak,} \\ \frac{1}{2g^2\epsilon_{II}} \left(\frac{H}{2\pi}\right)^2; & \text{peak,} \\ \frac{1}{2\epsilon_{II}} \left(\frac{H}{2\pi}\right)^2; & \text{UV part.} \end{cases} \quad (2.12)$$

A non-Gaussian tail was identified in this model through an analysis using the  $\delta N$  formalism [41]. The  $\delta N$  formalism connects the curvature perturbation  $\mathcal{R}$  at the end of inflation to the quantum fluctuations of the inflaton by evaluating the e-folding number backward during the superhorizon evolution of a Hubble patch from the end of inflation.

The  $\delta N$  calculation can be expressed as

$$\delta N = N_{\text{tot}}(\phi_i + \delta\phi, \Pi_i + \delta\Pi; \phi_{\text{end}}, \Pi_{\text{end}}) - N_{\text{tot}}(\phi_i, \Pi_i; \phi_{\text{end}}, \Pi_{\text{end}}), \quad (2.13)$$

where  $N_{\text{tot}} \equiv n_{\text{end}} - n_i > 0$  is counted backward to the end of inflation.

In the upward step model, a highly non-trivial non-Gaussian tail arises in the perturbation modes exiting the horizon near the step (i.e.,  $\phi \simeq \phi_*$ ) due to the non-linear dependence of  $\Pi(n)$  in (2.7). For modes that crossed the horizon much earlier, the attractor behavior of (2.10) suppresses the initial deviation of  $\Pi(n)$  from the attractor solution before the step. Thus,  $\delta N$  is primarily contributed by the linear part of (2.9),

$$\mathcal{R} = \delta N \simeq \frac{\delta\phi}{\sqrt{2\epsilon_I}}, \quad \text{long wave length modes.} \quad (2.14)$$

Based on the same argument, modes that exit the horizon long after the step, as well as long before the end of inflation, also follow a linear  $\delta N$  result:

$$\mathcal{R} \simeq \frac{\delta\phi}{\sqrt{2\epsilon_{II}}}, \quad \text{short wavelength modes.} \quad (2.15)$$

---

<sup>2</sup>Notably, this definition of  $h$  differs from [41] as we have absorbed the negative sign into the definition of  $\Pi$ .

However, for modes exiting the horizon just before the step, where  $n_c - n_i \ll 1$ , (2.10) implies

$$\delta\Pi_c \simeq \delta\Pi_i - 3\delta\phi, \quad (2.16)$$

meaning that the fluctuation of  $\phi_i$  affects the second slow-roll stage nonlinearly through  $\delta\Pi_d(\delta\phi)$ . For these modes, the e-folding number, counted backward from the end of inflation, is given by:

$$N_{\text{tot}} = N_I + N_{II} = (n_\star - n_i) + (n_{\text{end}} - n_\star). \quad (2.17)$$

Since  $N_I$  and  $N_{II}$  are evaluated using different solutions of (2.8), we cannot cancel  $n_\star$  between the two stages. Thus, two terms contribute to the final  $\delta N$ , with the nonlinearity arising from the  $\delta N_{II}$  part, which is our primary focus.

Setting  $X = II$  in (2.10),  $N_{II}$  is given by

$$N_{II} \equiv n_{\text{end}} - n_\star = \frac{1}{3\sqrt{2\epsilon_{II}}} [-3\phi_{\text{end}} + \Pi_{\text{end}} + 3C_{2,II}(\phi_\star, \Pi_d) - \sqrt{2\epsilon_{II}}]. \quad (2.18)$$

Substituting  $C_{2,II}(\phi_\star, \Pi_d)$  yields  $\delta N_{II}$ :

$$\delta N_{II} \simeq \frac{\Pi_d}{3\sqrt{2\epsilon_{II}}} \left[ \sqrt{1 - \frac{6}{g} \frac{\delta\phi}{\Pi_d} + 9 \left( \frac{\delta\phi}{\Pi_d} \right)^2} - 1 \right], \quad (2.19)$$

which agrees with the result in the small  $\eta_V$  limit found in [41]. Here, we focus on the case where  $g^2 h \ll 1$ , in which the curvature perturbation is dominated by the step effect. Thus,  $\mathcal{R}$  can be written as:

$$\mathcal{R} \simeq -\frac{2}{h} \left[ \sqrt{1 - h\mathcal{R}_G} - 1 \right], \quad (2.20)$$

where  $\mathcal{R}_G = 6\delta\phi/(gh\Pi_d)$  represents the linear part of (2.20).

This nonlinear  $\mathcal{R}$  results in a highly non-Gaussian tail in the PDF  $\mathbb{P}[\mathcal{R}]$ , which is challenging to achieve through perturbative methods. For example, when  $g^2 \ll 1$ , using the definition of the local non-Gaussianity parameter (1.1),  $f_{\text{NL}}$  in our model is given by:

$$f_{\text{NL}} \simeq \frac{5}{12} h > 0. \quad (2.21)$$

This result is also justified by applying the generalized consistency relation [47]. Since  $f_{\text{NL}}$  is the coefficient of the quadratic term, a positive  $f_{\text{NL}}$  increases the probability of a positive  $\mathcal{R}$ . From this perspective, it becomes clear that models with a positive  $f_{\text{NL}}$  are more likely to produce PBHs [47].

However, (2.20) imposes a cutoff on  $\mathcal{R}$ , meaning that the probability of  $\mathcal{R} > 2/h$  is zero, which deviates significantly from the Gaussian case. This cutoff suggests that PBHs formation must be considered more carefully when the non-Gaussian tail plays a significant role.

### 3 PBH formation in upward step model

#### 3.1 Basic setup for extended Press-Schechter formalism

The formation of PBHs is thought to occur due to the collapse of super-horizon fluctuations, which are large and rare when they reenter the horizon after inflation. Since the collapse

occurs in real space and is governed by the non-linearity of gravity, the full shape of the fluctuations must be known to determine whether a PBH will form. It has been shown that in the presence of non-Gaussianity, all orders of the correlators of curvature perturbation  $\langle \mathcal{R}\mathcal{R}\cdots\mathcal{R} \rangle$  are needed to describe the full profile of fluctuations [29, 67]. Compared to the curvature perturbation  $\mathcal{R}$ , the compaction function  $\mathcal{C}$  [68], which is defined as the mass excess relative to the background, serves as a more accurate estimator for the threshold of PBH formation [25, 26, 30, 69–71]. On super-horizon scales, assuming spherical symmetry, the compaction function  $\mathcal{C}$  during the radiation-dominated era can be expressed in terms of the curvature perturbation  $\mathcal{R}$  in the comoving gauge<sup>3</sup>:

$$\mathcal{C}(r) = \frac{2}{3}[1 - (1 + r\mathcal{R}'(r))^2] = \mathcal{C}_\ell - \frac{3}{8}\mathcal{C}_\ell^2, \quad (3.1)$$

where  $\mathcal{C}_\ell = -4r\mathcal{R}'/3$ , is referred to as the linear compaction function, and “ ’ ” denotes the derivative with respect to  $r$ .

Numerical results [72] show that the averaged compaction function  $\bar{\mathcal{C}}$  within a radius  $r_m$  is a reliable indicator of the collapse leading to PBH formation,

$$\bar{\mathcal{C}} \equiv \frac{3}{L^3(r_m)} \int_0^{L(r_m)} \mathcal{C}(r)L^2(r)dL, \quad (3.2)$$

where  $L(r, t) \equiv a(t)re^{\mathcal{R}(r, t)}$  is the so-called areal radius, and  $a(t)$  is the scale factor of the background. In the literature,  $r_m$  is chosen as the radius corresponding to the first local maximum of  $\mathcal{C}(r_m)$ .

When  $\bar{\mathcal{C}}$  exceeds a universal threshold, often set as  $\bar{\mathcal{C}}_{\text{th}} = 2/5$ , corresponding to  $\mathcal{C}_{\text{th}} = \mathcal{C}(r_m)$ , this region is believed to collapse into a PBH [72]. Using (3.1), we can convert  $\mathcal{C}_{\text{th}}$  to the linear compaction function  $\mathcal{C}_{\ell, \text{th}}$ . Here, we consider type I perturbations, where  $\mathcal{C}_\ell$  takes values in the range  $\mathcal{C}_{\ell, \text{th}} < \mathcal{C}_\ell < 4/3$ , corresponding to a monotonically increasing areal radius  $L(r)$ .

Given a profile of  $\mathcal{R}(r)$ , using the typical profile from *peak theory* [73–79], the type I local maximum  $\mathcal{C}(r_m)$  can be determined by the condition

$$\mathcal{R}' + r\mathcal{R}'' = 0. \quad (3.3)$$

Here, following the standard approach in the literature [73], and in the limit of high peaks,  $\nu = \mu/\sigma_0 \gg 1$  [79], we parametrize the profile of the Gaussian curvature perturbation in real space as

$$\mathcal{R}_G(r) = \mu\psi_0(r), \quad (3.4)$$

where

$$\psi_0(r) = \frac{1}{\sigma_0^2} \int \frac{dk}{k} \frac{\sin(kr)}{kr} \mathcal{P}_{\mathcal{R}_G}(k), \quad \sigma_0^2 = \int \frac{dk}{k} \mathcal{P}_{\mathcal{R}_G}(k). \quad (3.5)$$

The profile of the actual non-Gaussian curvature perturbation should also relate to the two-point function  $\mathcal{R}(r) \propto \langle \mathcal{R}(r_0 = 0)\mathcal{R}(r) \rangle$ , where  $\mathcal{R}(r_0)$  is the peak of the actual curvature perturbation and we take  $r_0 = 0$  as the center of the peak.

---

<sup>3</sup>In the literature, the curvature perturbation  $\zeta$ , defined in the uniform density gauge, is often used when discussing the compaction function. Since  $\zeta$  and  $\mathcal{R}$  are equivalent on super-horizon scales, for simplicity in notation, we use  $\mathcal{R}$  throughout this paper.



However, the nonlinear relation  $\mathcal{R} = \mathcal{F}[\mathcal{R}_G]$  implies that  $\langle \mathcal{R}(0)\mathcal{R}(r) \rangle \neq \mathcal{F}[\langle \mathcal{R}_G(0)\mathcal{R}_G(r) \rangle]$ . In this work, we do not adopt the traditional  $\mathcal{F}[\langle \mathcal{R}_G(0)\mathcal{R}_G(r) \rangle]$  approach to describe the profile of the non-Gaussian random field  $\mathcal{R}(\mathbf{x})$  in real space. Instead, we introduce a corrected two-point function  $\mathcal{P}_{\mathcal{R}}$  for this purpose. It should be emphasized that the main conclusions of our work are not affected by the specific parametrization of the profile. Generally, for a highly nonlinear  $\mathcal{F}$ , it is difficult to express  $\mathcal{P}_{\mathcal{R}}$  in terms of  $\mathcal{P}_{\mathcal{R}_G}$  analytically. However, since  $\mathcal{P}_{\mathcal{R}_G} \ll \mathcal{O}(1)$ , we expect that corrections from higher-order non-Gaussianity parameters will be suppressed by  $\mathcal{P}_{\mathcal{R}_G}^n$ . Thus the correction to the power spectrum of the non-Gaussian field can be calculated perturbatively, following the perturbative local non-Gaussian relation in (1.1),

$$\begin{aligned} \mathcal{P}_{\mathcal{R}}(\mathbf{k}) &= \mathcal{P}_{\mathcal{R}_G}(\mathbf{k}) \left( 1 + 3g_{\text{NL}} \langle \mathcal{R}_G^2(\mathbf{x}) \rangle + 6g_{\text{NL}}^2 \langle \mathcal{R}_G^2(\mathbf{x}) \rangle^2 + \dots \right) \\ &+ \frac{9k^3}{25\pi^2} f_{\text{NL}}^2 \int \frac{d^3\mathbf{p}}{(2\pi)^3} P_{\mathcal{R}_G}(\mathbf{p}) P_{\mathcal{R}_G}(\mathbf{k} - \mathbf{p}) \\ &+ \frac{3k^3}{\pi^2} g_{\text{NL}}^2 \int \int \frac{d^3\mathbf{l} d^3\mathbf{p}}{(2\pi)^6} P_{\mathcal{R}_G}(\mathbf{p}) P_{\mathcal{R}_G}(\mathbf{l}) P_{\mathcal{R}_G}(\mathbf{k} - \mathbf{l} - \mathbf{p}) \\ &+ \dots, \end{aligned} \quad (3.6)$$

where the  $\int \frac{d^3\mathbf{k}}{(2\pi)^3} P_{\mathcal{R}_G}(\mathbf{k}) e^{i\mathbf{k}\cdot\mathbf{r}} \equiv \langle \mathcal{R}_G(0)\mathcal{R}_G(r) \rangle$  defines the dimensionful power spectrum.

Substituting  $\mathcal{P}_{\mathcal{R}_G}$  in (3.4) and (3.5) with  $\mathcal{P}_{\mathcal{R}}$ , accounting for the correction from non-Gaussianity, allows us to parameterise the profile of the actual non-Gaussian curvature perturbation. Based on the standard process outlined above, we can determine the threshold  $\mathcal{C}_{\text{th}}$  to assess whether an overdense region satisfies the conditions for type-I PBH formation. The analytical expression for the threshold given in [80] provides a convenient way to determine the threshold  $\mathcal{C}_{\text{th}}$  in the model revisited in Section 2.

The core of the extended Press-Schechter formalism is calculating the probability distribution  $\mathbb{P}(\mathcal{C}_\ell)$  for the linear compaction function where  $\mathcal{C}_{\ell, \text{th}} < \mathcal{C}_\ell < 4/3$ . Let  $X = r\mathcal{R}'_G$ ,  $Y = \mathcal{R}_G$ , so that  $\mathcal{C}_\ell$  can be written as

$$\mathcal{C}_\ell = -\frac{4}{3} \mathcal{J}(Y) X, \quad (3.7)$$

where the Jacobian  $\mathcal{J}(Y) = d\mathcal{R} / d\mathcal{R}_G = \mathcal{F}'(\mathcal{R}_G)$ .

The two-dimensional joint probability distribution  $\mathbb{P}(X, Y)$  for  $X$  and  $Y$  is given by

$$\mathbb{P}(X, Y) = \frac{1}{2\pi\sqrt{\det(\boldsymbol{\Sigma})}} \exp\left(-\frac{\mathbf{V}^T \boldsymbol{\Sigma}^{-1} \mathbf{V}}{2}\right), \quad (3.8)$$

where  $\mathbf{V}^T = (X, Y)$ , and the covariance matrix  $\boldsymbol{\Sigma}$  is

$$\boldsymbol{\Sigma} = \begin{pmatrix} \Sigma_{XX} & \Sigma_{XY} \\ \Sigma_{XY} & \Sigma_{YY} \end{pmatrix}, \quad (3.9)$$

with each matrix element given by [27, 28]

$$\begin{aligned}\Sigma_{XX} &= \int d(\ln k)(kr)^2 \left[ \frac{dj_0}{dz}(kr) \right]^2 T^2(k, r) \mathcal{P}_{\mathcal{R}_G}(k) , \\ \Sigma_{XY} = \Sigma_{YX} &= \int d(\ln k)(kr) j_0(kr) \frac{dj_0}{dz}(kr) T^2(k, r) \mathcal{P}_{\mathcal{R}_G}(k) , \\ \Sigma_{YY} &= \int d(\ln k) j_0^2(kr) T^2(k, r) \mathcal{P}_{\mathcal{R}_G}(k) ,\end{aligned}\tag{3.10}$$

where  $j_0(z) = \sin(z)/z$ , and  $T(k, \tau)$  is the transfer function of the power spectrum during the radiation-dominated era

$$T(k, \tau) = 3 \frac{\sin(k\tau/\sqrt{3}) - (k\tau/\sqrt{3}) \cos(k\tau/\sqrt{3})}{(k\tau/\sqrt{3})^3} .\tag{3.11}$$

Note that  $r = \tau = r_m$  is used in the computation of  $\mathbb{P}(X, Y)$ .

And  $\mathcal{C}_\ell$  corresponds to probability  $\mathbb{P}(\mathcal{C}_\ell)$  as given in [28]:

$$\mathbb{P}(\mathcal{C}_\ell) = \int_{-\infty}^{+\infty} \frac{3}{4|\mathcal{J}(Y)|} \mathbb{P}\left(-\frac{3}{4} \frac{\mathcal{C}_\ell}{\mathcal{J}(Y)}, Y\right) dY .\tag{3.12}$$

Using  $\mathcal{C}_\ell$ , we can express the PBH mass spectrum as follows [77]:

$$\beta(M) d \ln M = \mathcal{K} \frac{[(\mathcal{C}_\ell - \frac{3}{8} \mathcal{C}_\ell^2) - \mathcal{C}_{\text{th}}]^{\gamma+1}}{\gamma (1 - \frac{3}{4} \mathcal{C}_\ell)} \mathbb{P}(\mathcal{C}_\ell) d \ln M ,\tag{3.13}$$

which accounts for critical collapse effects [81–88]:

$$M(\mathcal{C}_\ell) \sim \mathcal{K} \left[ \left( \mathcal{C}_\ell - \frac{3}{8} \mathcal{C}_\ell^2 \right) - \mathcal{C}_{\text{th}} \right]^\gamma M_H .\tag{3.14}$$

The relation between the current PBH abundance  $f(M)$  as a fraction of dark matter and their initial abundance  $\beta(M)$  is given by [77]:

$$f(M) = \frac{\Omega_m h^2}{\Omega_{\text{DM}} h^2} \frac{T_{r_m}}{T_{\text{eq}}} \beta(M) .\tag{3.15}$$

We use the relationship between temperature  $T$  and wave number  $k$  from [89], and the fitted formulae for the number of degrees of freedom at different temperatures in [90], to jointly give the conversion factor between  $f(M)$  and  $\beta(M)$ . The current total PBH abundance as a fraction of dark matter is then given by

$$f_{\text{PBH}} = \int_0^{M_{\text{max}}} f(M) d \ln M .\tag{3.16}$$

### 3.2 PBH abundance

By utilizing the extended Press-Schechter formalism, we find that non-Gaussianity affects the abundance of PBHs primarily in two aspects, both stemming from the nonlinear relation  $\mathcal{R} = \mathcal{F}[\mathcal{R}_G]$ :

- The first effect is on the configuration of the actual curvature perturbation in real space,  $\mathcal{R}(r)$ , which can deviate from the Gaussian case. As shown in (3.6), the two-point function, which mainly determines the profile around the peak, is generally not significantly affected. However, due to the nonlinearity in (2.20), there is a cut-off for  $\mathcal{R}_G$ , which also imposes a cut-off in the compaction function  $\mathcal{C}(r)$ . This leads to changes in  $r_m$  and the threshold  $\mathcal{C}_{\text{th}}$ , thereby altering the probability distribution  $\mathbb{P}(X, Y)$ .
- The second effect arises directly from the non-trivial integration path introduced by the nonlinear relation (3.7) when calculating the probability  $\mathbb{P}(\mathcal{C}_\ell)$  using (3.12). This path influences how non-Gaussianity impacts PBH abundance through the modified probability space.

To understand the effects of the non-Gaussian tail arising from (2.20), we compute the PBH abundance using the extended Press-Schechter formalism in a concrete model shown in Figure 1.

Using the same parameters as in Figure 1, one can solve the Sasaki-Mukhanov equation numerically to calculate the power spectrum  $\mathcal{P}_{\mathcal{R}_G}(k)$  at the end of inflation,

$$\frac{d^2 \mathcal{R}_{G,k}}{d\tau^2} + 2 \frac{1}{z} \frac{dz}{d\tau} \frac{d\mathcal{R}_{G,k}}{d\tau} + k^2 \mathcal{R}_{G,k} = 0, \quad (3.17)$$

where  $d\tau = dt/a$  is the conformal time and  $z \equiv ad\phi/dn$ . As discussed in Section 2 and (2.12), the power spectrum is enhanced due to the rapid decrease in  $\Pi$ . A broken power-law (BPL) function (3.18) can effectively describe the peak behavior of  $\mathcal{P}_{\mathcal{R}_G}(k)$ , as shown in Figure 2.

Next, we will estimate the PBH abundance in this model based on the BPL parameterized power spectrum,

$$\mathcal{P}_{\mathcal{R}_G}^{\text{BPL}}(k) = A \frac{(\alpha + \beta)^\gamma}{\left[ \beta (k/k_*)^{-\alpha/\gamma} + \alpha (k/k_*)^{\beta/\gamma} \right]^\gamma}. \quad (3.18)$$

Since PBH formation is primarily determined by the peak of the power spectrum, this approximation does not affect the results of our analysis much.

By employing the extended Press-Schechter formalism outlined in Section 3.1, we find that the abundance of PBHs from the type-I channel is significantly suppressed by the non-Gaussian tail described by (2.20). To understand how the non-Gaussian tail, controlled by  $h$ , affects  $f_{\text{PBH}}$ , we compute  $f_{\text{PBH}}$  for different values of  $h$ , keeping  $\mathcal{P}_{\mathcal{R}_G}(k)$  fixed to the BPL spectrum shown in Figure 2. And we perturbatively estimate the non-Gaussian correction to  $\mathcal{P}_{\mathcal{R}}(k)$  by using (3.6) as shown in Figure 3:

As shown in Figure 4, as  $h$  increases from  $h = 0$ ,  $f_{\text{PBH}}$  is initially enhanced by the non-Gaussian tail compared to the Gaussian case ( $h = 0$ ). For the  $\mathcal{P}_{\mathcal{R}_G}(k)$  in Figure 2, PBHs are overproduced in the Gaussian scenario. However, as  $h$  increases beyond approximately  $h \simeq 5.9$ ,  $f_{\text{PBH}}$  drops by a factor of  $10^{52}$  and then begins to rise again.

The sharp drop in  $f_{\text{PBH}}$  around  $h \simeq 5.9$  is not unexpected. We can explain this, even with a rough estimate, as anticipated in previous studies [41]. Since the averaged density contrast is proportional to the curvature perturbation at horizon crossing,  $\mathcal{R}_{\text{th}} \sim \mathcal{O}(1)$  serves as a rough criterion for PBH formation. However, the non-linear relation (2.20) implies a cut-off at  $2/h$  in the PDF of  $\mathcal{R}$ . Using the extended Press-Schechter formalism, we confirm this naive argument.

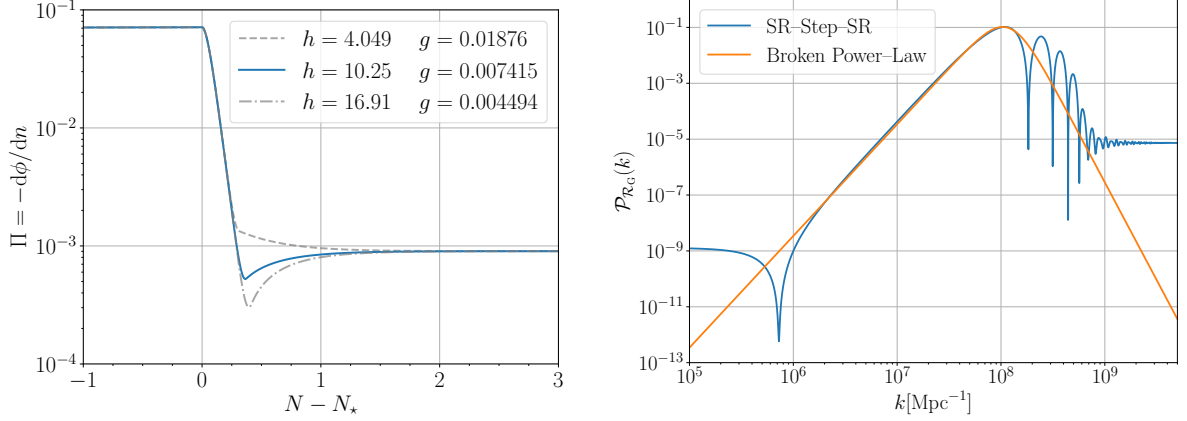


**Figure 2.** **Left panel:** The evolution of the inflaton velocity  $\Pi(n)$  near the step. The sharp upward step significantly reduces  $\Pi(n)$  within 0.5 e-folds. Changing  $\Delta V$  results in different curves, each corresponding to different values of  $g$  and  $h$ . The blue line corresponds to the potential shown in Figure 1. **Right panel:** The dimensionless power spectrum  $\mathcal{P}_{\mathcal{R}_G}(k)$  for the model with the potential from Figure 1. A BPL parametrized by (3.18) with  $A = 0.104$ ,  $\alpha = 4$ ,  $\gamma = 3$ ,  $\beta = 7$ , and  $k_* = 1.04 \times 10^8 \text{ Mpc}^{-1}$  fits the result well.

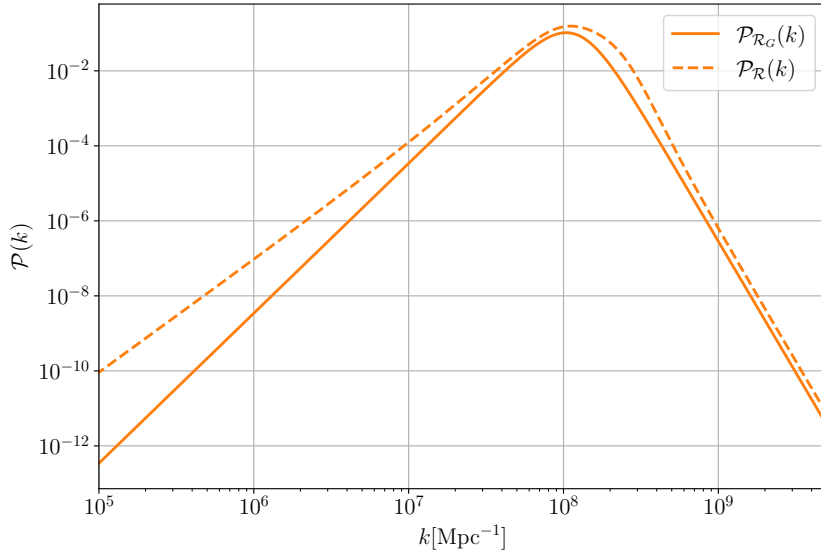


**Figure 3.** The comparison of  $\mathcal{P}_{\mathcal{R}}(k)$  with non-Gaussian correction from (3.6) and BPL  $\mathcal{P}_{\mathcal{R}_G}(k)$  from the right panel of Figure 2.

From the perspective of extended Press-Schechter formalism, the sudden drop of  $f_{\text{PBH}}$  can be seen as the evidence for type-II fluctuation of PBHs. We show the profile of compaction function  $\mathcal{C}(r)$  of non-Gaussian curvature perturbation  $\mathcal{R}(r)$  utilized by different  $\mu$  in Section 3.1 with different  $h$  to understand it clearly. As discussed in Section 3.1, we increase  $\mu$  from a small initial value to find  $\mathcal{C}_{\text{th}} = \mathcal{C}(r_m)$ , where  $\mathcal{C}$  reaches a local maximum at  $r_m$ . This  $r_m$  also determines the joint PDF  $\mathbb{P}(X, Y)$  via (3.10). The nonlinear relation (2.20) introduces a cut-off for  $\mathcal{R}_G$ , leading to a cut-off and a corresponding type-II peak in  $\mathcal{C}(r)$  when  $\mu$  is large.

As shown in Figure 5, when  $\mu$  is small, the first peak in  $\mathcal{C}(r)$  corresponds to a standard type-I peak, consistent with (3.3). However, for larger values of  $\mu$ ,  $\mathcal{C}(r)$  with larger  $h$  results

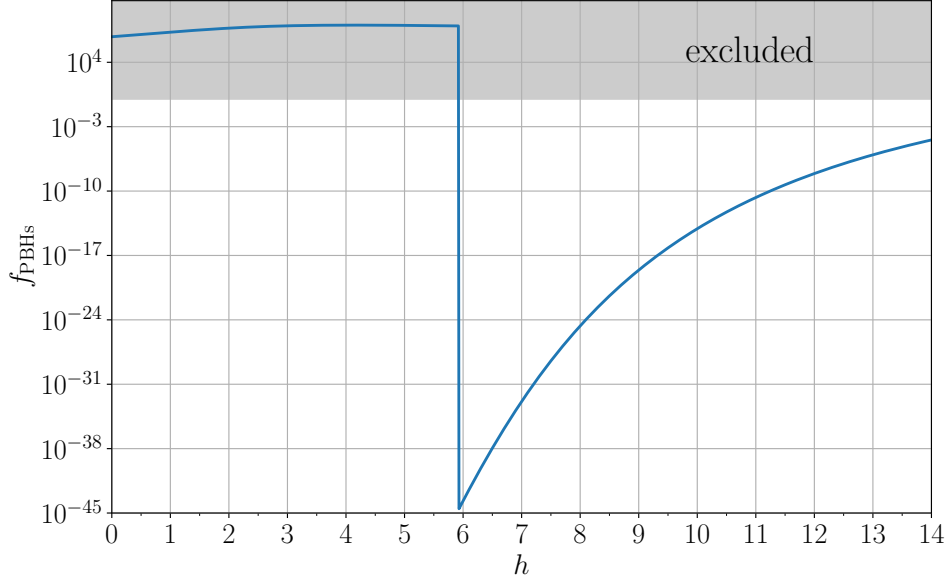


**Figure 4.** With the given BPL power spectrum, the abundance of PBHs from the type-I channel is evaluated for various  $h$  values, considering the impact of the non-Gaussian tail. When  $h < 5.9$ , the non-Gaussianity introduced by (2.20) enhances PBH formation. However, when  $h > 5.9$ , the cutoff effect of (2.20) leads to a sharp reduction in the PBH abundance from the type-I channel. As  $h$  increases further,  $f_{\text{PBH}}$  begins to rise again, but at this point, a more precise calculation for the type-II channel is likely necessary.

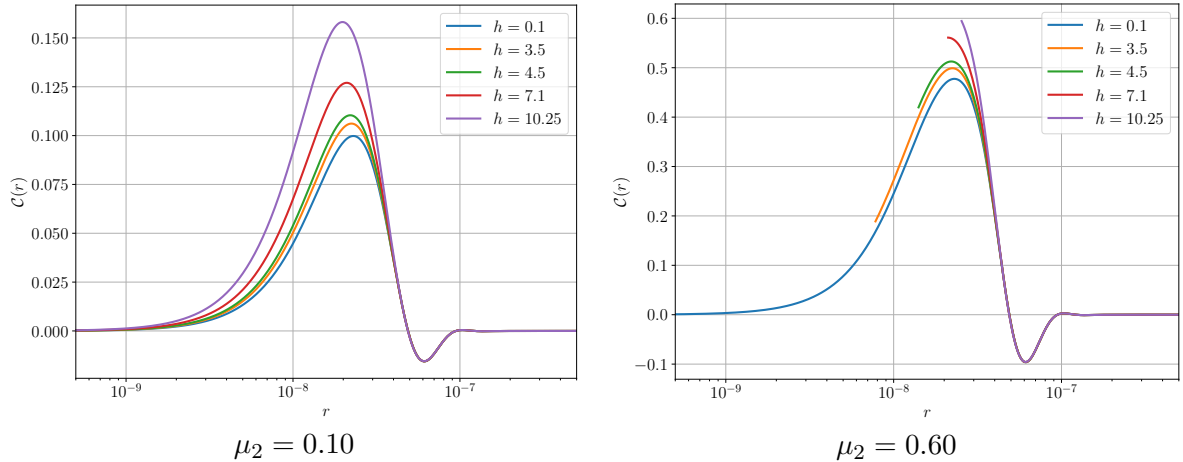


**Figure 5.** The  $\mathcal{C}(r)$  profiles for different  $h$  values with two given  $\mu$  values. We increase  $\mu$  to determine the threshold  $\mathcal{C}_{\text{th}}$  and  $r_{\text{m}}$ .

in a cut-off, as seen in the right panel of Figure 5. When this cut-off eliminates the first type-I peak, the next type-I peak can be found at larger  $r$ .

In practical calculations using the extended Press-Schechter formalism, we find next type-I local maximum, causing  $r_{\text{m}}$  to increase discontinuously. In this case, PBH formation via the type-I channel is significantly suppressed. For larger  $h$ , which corresponds to a smaller cut-off in  $\mathbb{P}[\mathcal{R}]$ , the sudden change in  $r_{\text{m}}$  occurs with a smaller  $\mu$ . After this sudden shift, the  $r_{\text{m}}$  corresponding to the type-I peak becomes almost insensitive to changes in  $h$ .

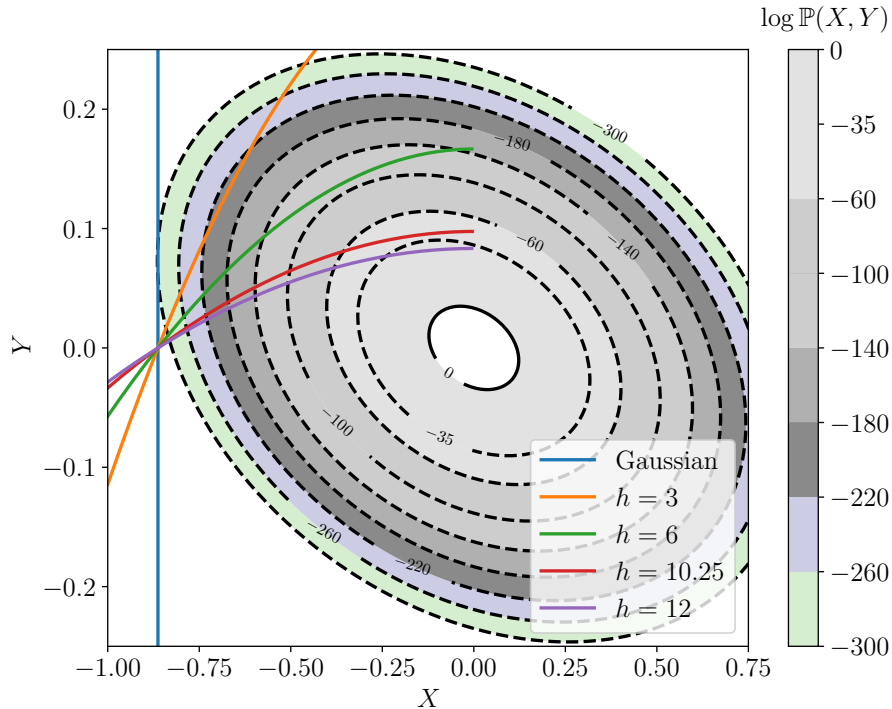


**Figure 6.** The integration paths for calculating  $\mathbb{P}(\mathcal{C}_\ell)$  corresponding to different  $h$  values, with  $\mathcal{C}_\ell = 1.15$ . When the impact of non-Gaussianity on  $\mathbb{P}(X, Y)$  is small, we can roughly estimate the PBH production by considering different integration paths in (3.7). The PDF  $\mathbb{P}(X, Y)$  shown in the figure corresponds to  $h = 10.25$ .

Therefore, we can approximately assume that after the abrupt change in  $r_m$ , further increases in  $h$  have little impact on  $\mathbb{P}(X, Y)$ . However, different  $h$  values also affect the integral path in (3.12). For a given PDF  $\mathbb{P}(X, Y)$ , larger  $h$  shifts the integral path through regions of higher probability, as shown in Figure 6. This explains the increasing  $f_{\text{PBH}}$  in Figure 4 when  $h > 5.9$ . However, it is important to emphasize that when  $h > 5.9$ , the sudden drop in  $f_{\text{PBH}}$  indicates that PBHs formed via type-I fluctuations are suppressed, while the type-II channel may become more significant in this regime [91, 92].

Estimating the formation of PBHs from Type-II fluctuations is challenging not only due to the complexity arising from the non-monotonic behavior of the areal radius  $L(r)$ , but also because the mass associated with these fluctuations can be significantly larger than that of the Hubble patch. For modes exiting the horizon just before the step, there is a possibility that the inflaton becomes trapped at the bottom of the step due to large quantum fluctuations. This phenomenon directly leads to the cut-off for  $\mathcal{R}_G$  in (2.20).

Nevertheless, we can approximately estimate the probability of the inflaton being trapped as

$$\mathbb{P}\left(\mathcal{R}_G > \frac{1}{h}\right) = \int_{1/h}^{+\infty} \frac{1}{\sqrt{2\pi\sigma_{\mathcal{R}_G}^2}} \exp\left(-\frac{\mathcal{R}_G^2}{2\sigma_{\mathcal{R}_G}^2}\right) d\mathcal{R}_G, \quad (3.19)$$

where  $\sigma_{\mathcal{R}_G}^2 = \Sigma_{YY}$ , as derived in Section 3.1. For the parameters used in the right panel of Figure 2, this probability is extremely low, of the order  $\mathcal{O}(10^{-23})$ .

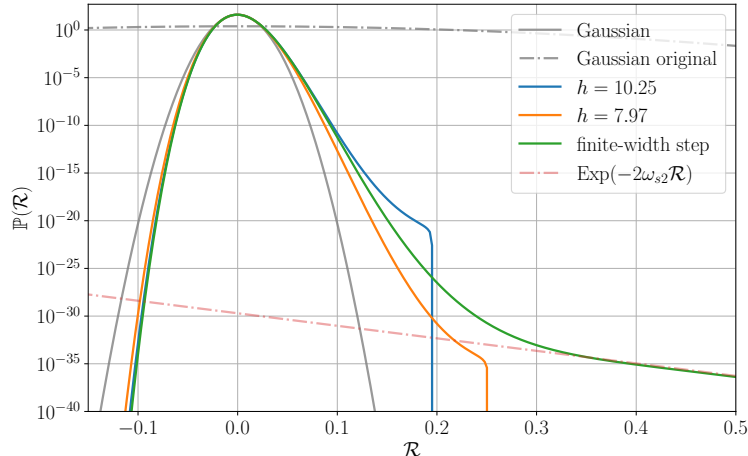


**Figure 7.** The PDF  $\mathbb{P}[\mathcal{R}]$  for modes exiting the horizon just before the upward step is shown. The green line exhibits an exponential tail with  $\omega_{s2} \simeq 15.13$ , accounting for the finite size effects of the upward step [61]. Two Gaussian distributions are present in this figure: the variance of the broader one corresponds precisely to the variance of  $\mathcal{R}_G$  as described in (2.20). However, as discussed earlier, when cut-off eliminates the first type-I peak, a sudden increase in  $r_m$  modifies the variance  $\sigma_{\mathcal{R}_G}^2$ . The variance of the narrower Gaussian is determined by this new  $r_m$ .

The model used in Figure 1, which generates the power spectrum shown in the right panel of Figure 2, does not feature an infinitely sharp upward step. Only in the case of an extremely sharp step (2.7) can hold, but in such cases, the power spectrum  $\mathcal{P}_{\mathcal{R}_G}(k)$  would oscillate and fail to decay to the second slow-roll solution. For a step with finite width, (2.7) needs to be modified to account for the Hubble friction as the inflaton crosses the step [61], although the nonlinear relationship between  $\Pi_c$  and  $\Pi_d$  remains.

As shown in Figure 7, the finite width of the step removes the hard cut-off in the PDF of  $\mathcal{R}$ , instead producing an exponentially decaying tail  $\mathbb{P}[\mathcal{R}] \propto \exp(-2\omega_{s2}\mathcal{R})$ , where the index  $\omega_{s2} \simeq \sqrt{2} \Pi_c / \Delta\phi$  is determined by the step width. In our case, we find  $\omega_{s2} \simeq 15.13$ , which does not alter the key conclusions. This exponential tail results in an “equivalent”  $10.25 > h > 7.97$ , meaning that the abundance of type-I PBHs from the realistic model without a cut-off is the same as with a modified  $10.25 > h > 7.97$ .

Additionally, we find that the abundance of PBHs in models with an upward step is highly sensitive to the parameters. A wider step or even a change in the shape of the step can significantly affect the results [91].

## 4 Implications for indirect observations of PBHs

Observing the primordial power spectrum through gravitational waves and CMB  $\mu$ -distortion to constrain PBH abundance is considered an indirect method. Since the abundance of PBHs in the presence of non-Gaussianity cannot be fully determined by the power spectrum, it introduces significant uncertainty to such indirect observations.

### 4.1 Energy density spectrum of SIGWs

For instance, based on PTAs observations of the stochastic gravitational wave background [11–19], if we assume that the entire stochastic background is generated by primordial scalar perturbations, as shown in the right panel of Figure 2, the observations imply that  $\mathcal{P}_{\mathcal{R}_G}(k) \sim$

$\mathcal{O}(10^{-1})$ . At the same time, Figure 4 shows that PBHs are overproduced in the Gaussian case ( $h = 0$ ).

When examining the impact of non-Gaussianity on PBH abundance, a polynomial series expansion (1.1) usually indicates that a positive  $f_{\text{NL}}$  always increases the abundance of PBHs. This reasoning suggests that models with an upward step are disfavored by PTAs observations since they exacerbate the overproduction of PBHs [47].

However, when we consider the effect of non-perturbative non-Gaussianity (2.20), we find that the issue of overproduction can be resolved, although fine-tuning is required. Using the power spectrum from the right panel of Figure 2, we apply the standard approach to compute the present-day energy spectrum of SIGWs,  $\Omega_{\text{GW}}(\eta_0, k)$ , and include corrections up to  $f_{\text{NL}}^2$  order due to non-Gaussianity [93–99]. As shown in Figure 8, the SIGWs produced in the upward step model align well with the NANOGrav 15-year data without leading to an overproduction of PBHs.

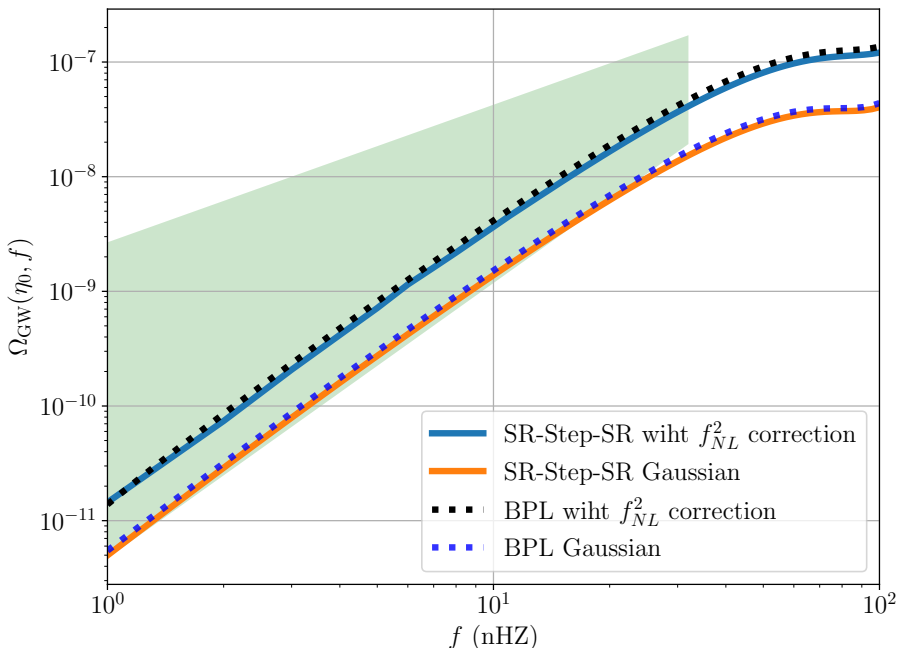


**Figure 8.** Based on our model, we compute the energy spectrum  $\Omega_{\text{GW}}(\eta_0, k)$  using the power spectrum shown in the right panel of Figure 2. Additionally, we account for the correction from  $f_{\text{NL}}^2$  to  $\Omega_{\text{GW}}(\eta_0, k)$ . The green shaded regions represent the  $2\sigma$  confidence interval as indicated by the NANOGrav 15-year data.

## 5 Conclusion

In this work, we have investigated the formation of PBHs within the framework of an upward step inflationary model. A key finding is that the nonlinear relation between the curvature perturbation and the field fluctuation,  $\mathcal{R}(\delta\phi) = \mathcal{F}[\mathcal{R}_G]$ , introduces a cutoff that deviates significantly from the Gaussian case, necessitating a reevaluation of PBH formation mechanisms. This necessitates a careful reevaluation of PBH formation mechanisms, as the curvature perturbation  $\mathcal{R}$  is not the appropriate variable for calculating the abundance of PBHs [69–71].



By employing the extended Press-Schechter formalism, we demonstrate that non-Gaussianity significantly influences PBH formation through the nonlinear relation between the curvature perturbation and its Gaussian counterpart. This nonlinearity introduces a cut-off in the curvature perturbation, which impacts PBH formation in two key ways:

First, it modifies the compaction function  $\mathcal{C}(r)$ , leading to changes in the characteristic scale  $r_m$ , the threshold  $\mathcal{C}_{\text{th}}$ , and the probability distribution  $\mathbb{P}(X, Y)$ . Second, the nonlinear relation affects the integration path used to compute the probability  $\mathbb{P}(\mathcal{C}_\ell)$ , altering the estimation of PBH abundance by influencing the regions of integration in probability space. Consequently, the formation of PBHs, particularly through the type-I channel, is highly sensitive to this non-Gaussian correction.

Our results show that as the non-Gaussian parameter  $h$  increases, the PBH fraction  $f_{\text{PBH}}$  initially increases compared to the Gaussian case. However, beyond a critical value of  $h \simeq 5.9$ ,  $f_{\text{PBH}}$  sharply declines before gradually increasing again. This behavior is due to the cutoff in the probability distribution function of  $\mathcal{R}$  induced by the nonlinear relation, effectively suppressing PBH formation via the type-I channel when  $h$  exceeds the critical value.

This study has significant implications for indirect observations of PBHs through gravitational waves and CMB  $\mu$ -distortions. In the presence of non-Gaussianity, the abundance of PBHs cannot be fully determined by the power spectrum alone, introducing significant uncertainty to such indirect observations. For instance, based on PTAs observations, if we assume that the entire stochastic gravitational wave background is generated by primordial scalar perturbations, the observations imply a large amplitude of  $\mathcal{P}_{\mathcal{R}_G}(k) \sim \mathcal{O}(10^{-1})$ . In the Gaussian case, this would lead to an overproduction of PBHs. However, considering the effect of non-perturbative non-Gaussianity, the overproduction issue can be resolved, aligning the model with current observations without conflicting with PBH constraints.

Our findings highlight that strong non-Gaussian features can significantly impact the interpretation of indirect PBH observations. This underscores the necessity of incorporating non-Gaussian effects into theoretical models and observational analyses to accurately predict PBH abundances and interpret gravitational wave data.

In conclusion, this study emphasizes the crucial role of non-Gaussianity in PBH formation and its implications for indirect observational constraints. The upward step model demonstrates how non-Gaussian features can mitigate the overproduction of PBHs without conflicting with current observations. In future work, investigation of type-II fluctuations in such models using numerical simulation methods may provide deeper insights into PBH formation mechanisms and their observational signatures.

## Acknowledgments

We thank Albert Escrivà, Gabriele Franciolini, Xin-Chen He, Kaloian Dimitrov Lozanov, Shi Pi, Misao Sasaki, Xinpeng Wang, Qiyue Xia, Shuichiro Yokoyama, Chul-Moon Yoo, and Dongdong Zhang for valuable discussions. This work is supported in part by the National Key R&D Program of China (2021YFC2203100), by NSFC (12261131497), by CAS young interdisciplinary innovation team (JCTD-2022-20), by 111 Project (B23042), by Fundamental Research Funds for Central Universities, by CSC Innovation Talent Funds, by USTC Fellowship for International Cooperation, by USTC Research Funds of the Double First-Class Initiative, by the National Key Research and Development Program of China (2021YFC2203203), and by the Science and Technology Plan Projects of the Tibet Au-

tonomous Region (XZ202102YD0029C). It is also supported in part by the JSPS KAKENHI grants No. 20H05853 and 24K00624.

We would also like to express our sincere gratitude to the Dynamics of Primordial Black Hole Formation II (DPBHF2) workshop held in Nagoya, which provided valuable insights and greatly contributed to the progress of this work.

## References

- [1] S. Hawking, *Gravitationally collapsed objects of very low mass*, *Mon. Not. Roy. Astron. Soc.* **152** (1971) 75.
- [2] B.J. Carr and S.W. Hawking, *Black holes in the early Universe*, *Mon. Not. Roy. Astron. Soc.* **168** (1974) 399.
- [3] B.J. Carr, *The Primordial black hole mass spectrum*, *Astrophys. J.* **201** (1975) 1.
- [4] B. Carr and F. Kuhnel, *Primordial Black Holes as Dark Matter: Recent Developments*, *Ann. Rev. Nucl. Part. Sci.* **70** (2020) 355 [2006.02838].
- [5] A.D. Dolgov, *Tension between HST/JWST and  $\Lambda$ CDM Cosmology, PBH, and Antimatter in the Galaxy*, in *14th Frascati workshop on Multifrequency Behaviour of High Energy Cosmic Sources*, 10, 2023 [2310.00671].
- [6] LIGO SCIENTIFIC, VIRGO collaboration, *Observation of Gravitational Waves from a Binary Black Hole Merger*, *Phys. Rev. Lett.* **116** (2016) 061102 [1602.03837].
- [7] LIGO SCIENTIFIC, VIRGO collaboration, *GW151226: Observation of Gravitational Waves from a 22-Solar-Mass Binary Black Hole Coalescence*, *Phys. Rev. Lett.* **116** (2016) 241103 [1606.04855].
- [8] LIGO SCIENTIFIC, VIRGO collaboration, *GW170104: Observation of a 50-Solar-Mass Binary Black Hole Coalescence at Redshift 0.2*, *Phys. Rev. Lett.* **118** (2017) 221101 [1706.01812].
- [9] LIGO SCIENTIFIC, VIRGO collaboration, *GW170814: A Three-Detector Observation of Gravitational Waves from a Binary Black Hole Coalescence*, *Phys. Rev. Lett.* **119** (2017) 141101 [1709.09660].
- [10] LIGO SCIENTIFIC, VIRGO collaboration, *GW170608: Observation of a 19-solar-mass Binary Black Hole Coalescence*, *Astrophys. J. Lett.* **851** (2017) L35 [1711.05578].
- [11] NANOGrav collaboration, *The NANOGrav 15 yr Data Set: Evidence for a Gravitational-wave Background*, *Astrophys. J. Lett.* **951** (2023) L8 [2306.16213].
- [12] NANOGrav collaboration, *The NANOGrav 15 yr Data Set: Observations and Timing of 68 Millisecond Pulsars*, *Astrophys. J. Lett.* **951** (2023) L9 [2306.16217].
- [13] EPTA, INPTA: collaboration, *The second data release from the European Pulsar Timing Array - III. Search for gravitational wave signals*, *Astron. Astrophys.* **678** (2023) A50 [2306.16214].
- [14] EPTA collaboration, *The second data release from the European Pulsar Timing Array - I. The dataset and timing analysis*, *Astron. Astrophys.* **678** (2023) A48 [2306.16224].
- [15] EPTA collaboration, *The second data release from the European Pulsar Timing Array: V. Implications for massive black holes, dark matter and the early Universe*, 2306.16227.
- [16] D.J. Reardon et al., *Search for an Isotropic Gravitational-wave Background with the Parkes Pulsar Timing Array*, *Astrophys. J. Lett.* **951** (2023) L6 [2306.16215].
- [17] A. Zic et al., *The Parkes Pulsar Timing Array Third Data Release*, 2306.16230.

- [18] D.J. Reardon et al., *The Gravitational-wave Background Null Hypothesis: Characterizing Noise in Millisecond Pulsar Arrival Times with the Parkes Pulsar Timing Array*, *Astrophys. J. Lett.* **951** (2023) L7 [2306.16229].
- [19] H. Xu et al., *Searching for the Nano-Hertz Stochastic Gravitational Wave Background with the Chinese Pulsar Timing Array Data Release I*, *Res. Astron. Astrophys.* **23** (2023) 075024 [2306.16216].
- [20] M. He, K. Kohri, K. Mukaida and M. Yamada, *Formation of hot spots around small primordial black holes*, *JCAP* **01** (2023) 027 [2210.06238].
- [21] PLANCK collaboration, *Planck 2018 results. VI. Cosmological parameters*, *Astron. Astrophys.* **641** (2020) A6 [1807.06209].
- [22] NANOGrav collaboration, *The NANOGrav 15 yr Data Set: Search for Signals from New Physics*, *Astrophys. J. Lett.* **951** (2023) L11 [2306.16219].
- [23] J. Ellis, M. Fairbairn, G. Franciolini, G. Hütsi, A. Iovino, M. Lewicki et al., *What is the source of the PTA GW signal?*, *Phys. Rev. D* **109** (2024) 023522 [2308.08546].
- [24] G. Franciolini, A. Iovino, Junior., V. Vaskonen and H. Veermae, *Recent Gravitational Wave Observation by Pulsar Timing Arrays and Primordial Black Holes: The Importance of Non-Gaussianities*, *Phys. Rev. Lett.* **131** (2023) 201401 [2306.17149].
- [25] T. Harada, C.-M. Yoo, T. Nakama and Y. Koga, *Cosmological long-wavelength solutions and primordial black hole formation*, *Phys. Rev. D* **91** (2015) 084057 [1503.03934].
- [26] I. Musco, *Threshold for primordial black holes: Dependence on the shape of the cosmological perturbations*, *Phys. Rev. D* **100** (2019) 123524 [1809.02127].
- [27] S. Young, *Peaks and primordial black holes: the effect of non-Gaussianity*, *JCAP* **05** (2022) 037 [2201.13345].
- [28] A.D. Gow, H. Assadullahi, J.H.P. Jackson, K. Koyama, V. Vennin and D. Wands, *Non-perturbative non-Gaussianity and primordial black holes*, *EPL* **142** (2023) 49001 [2211.08348].
- [29] G. Ferrante, G. Franciolini, A. Iovino, Junior. and A. Urbano, *Primordial non-Gaussianity up to all orders: Theoretical aspects and implications for primordial black hole models*, *Phys. Rev. D* **107** (2023) 043520 [2211.01728].
- [30] T. Harada, C.-M. Yoo and Y. Koga, *Revisiting compaction functions for primordial black hole formation*, *Phys. Rev. D* **108** (2023) 043515 [2304.13284].
- [31] G. Ferrante, G. Franciolini, A. Iovino, Junior. and A. Urbano, *Primordial black holes in the curvaton model: possible connections to pulsar timing arrays and dark matter*, *JCAP* **06** (2023) 057 [2305.13382].
- [32] L. Liu, Z.-C. Chen and Q.-G. Huang, *Implications for the non-Gaussianity of curvature perturbation from pulsar timing arrays*, [2307.01102](#).
- [33] S. Choudhury, K. Dey, A. Karde, S. Panda and M. Sami, *Primordial non-Gaussianity as a saviour for PBH overproduction in SIGWs generated by Pulsar Timing Arrays for Galileon inflation*, [2310.11034](#).
- [34] A.J. Iovino, G. Perna, A. Riotto and H. Veermäe, *Curbing PBHs with PTAs*, *JCAP* **10** (2024) 050 [2406.20089].
- [35] S. Choudhury, K. Dey, S. Ganguly, A. Karde, S.K. Singh and P. Tiwari, *Negative non-Gaussianity as a salvager for PBHs with PTAs in bounce*, [2409.18983](#).
- [36] G. Franciolini, A. Kehagias, S. Matarrese and A. Riotto, *Primordial Black Holes from Inflation and non-Gaussianity*, *JCAP* **03** (2018) 016 [1801.09415].

- [37] G. Panagopoulos and E. Silverstein, *Primordial Black Holes from non-Gaussian tails*, [1906.02827](#).
- [38] D.G. Figueroa, S. Raatikainen, S. Rasanen and E. Tomberg, *Non-Gaussian Tail of the Curvature Perturbation in Stochastic Ultraslow-Roll Inflation: Implications for Primordial Black Hole Production*, *Phys. Rev. Lett.* **127** (2021) 101302 [[2012.06551](#)].
- [39] A. Achucarro, S. Cespedes, A.-C. Davis and G.A. Palma, *The hand-made tail: non-perturbative tails from multifield inflation*, *JHEP* **05** (2022) 052 [[2112.14712](#)].
- [40] L.-Y. Chen, H. Yu and P. Wu, *Primordial non-Gaussianity in inflation with gravitationally enhanced friction*, *Phys. Rev. D* **106** (2022) 063537 [[2210.05201](#)].
- [41] Y.-F. Cai, X.-H. Ma, M. Sasaki, D.-G. Wang and Z. Zhou, *Highly non-Gaussian tails and primordial black holes from single-field inflation*, *JCAP* **12** (2022) 034 [[2207.11910](#)].
- [42] T. Nakama and T. Suyama, *Primordial black holes as a novel probe of primordial gravitational waves*, *Phys. Rev. D* **92** (2015) 121304 [[1506.05228](#)].
- [43] V. Dandoy, V. Domcke and F. Rompineve, *Search for scalar induced gravitational waves in the international pulsar timing array data release 2 and NANOgrav 12.5 years datasets*, *SciPost Phys. Core* **6** (2023) 060 [[2302.07901](#)].
- [44] K. Inomata, K. Kohri and T. Terada, *Detected stochastic gravitational waves and subsolar-mass primordial black holes*, *Phys. Rev. D* **109** (2024) 063506 [[2306.17834](#)].
- [45] Y.-F. Cai, X.-C. He, X.-H. Ma, S.-F. Yan and G.-W. Yuan, *Limits on scalar-induced gravitational waves from the stochastic background by pulsar timing array observations*, *Sci. Bull.* **68** (2023) 2929 [[2306.17822](#)].
- [46] S. Wang, Z.-C. Zhao, J.-P. Li and Q.-H. Zhu, *Implications of pulsar timing array data for scalar-induced gravitational waves and primordial black holes: Primordial non-Gaussianity fNL considered*, *Phys. Rev. Res.* **6** (2024) L012060 [[2307.00572](#)].
- [47] H. Firouzjahi and A. Riotto, *Sign of non-Gaussianity and the primordial black holes abundance*, *Phys. Rev. D* **108** (2023) 123504 [[2309.10536](#)].
- [48] L. Covi, J. Hamann, A. Melchiorri, A. Slosar and I. Sorbera, *Inflation and WMAP three year data: Features have a Future!*, *Phys. Rev. D* **74** (2006) 083509 [[astro-ph/0606452](#)].
- [49] J. Hamann, L. Covi, A. Melchiorri and A. Slosar, *New Constraints on Oscillations in the Primordial Spectrum of Inflationary Perturbations*, *Phys. Rev. D* **76** (2007) 023503 [[astro-ph/0701380](#)].
- [50] M.J. Mortonson, C. Dvorkin, H.V. Peiris and W. Hu, *CMB polarization features from inflation versus reionization*, *Phys. Rev. D* **79** (2009) 103519 [[0903.4920](#)].
- [51] P. Adshead, C. Dvorkin, W. Hu and E.A. Lim, *Non-Gaussianity from Step Features in the Inflationary Potential*, *Phys. Rev. D* **85** (2012) 023531 [[1110.3050](#)].
- [52] V. Miranda and W. Hu, *Inflationary Steps in the Planck Data*, *Phys. Rev. D* **89** (2014) 083529 [[1312.0946](#)].
- [53] V. Miranda, W. Hu, C. He and H. Motohashi, *Nonlinear Excitations in Inflationary Power Spectra*, *Phys. Rev. D* **93** (2016) 023504 [[1510.07580](#)].
- [54] K. Kefala, G.P. Kodaxis, I.D. Stamou and N. Tetradis, *Features of the inflaton potential and the power spectrum of cosmological perturbations*, *Phys. Rev. D* **104** (2021) 023506 [[2010.12483](#)].
- [55] I. Wolfson, *Analytic correlation of inflationary potential to power spectrum shape: limits of validity, and ‘no-go’ for small field model analytics*, *JCAP* **01** (2022) 036 [[2110.10557](#)].
- [56] S.S. Mishra and V. Sahni, *Primordial Black Holes from a tiny bump/dip in the Inflaton potential*, *JCAP* **04** (2020) 007 [[1911.00057](#)].

- [57] K. Inomata, E. McDonough and W. Hu, *Primordial black holes arise when the inflaton falls*, *Phys. Rev. D* **104** (2021) 123553 [[2104.03972](#)].
- [58] I. Dalianis, G.P. Kodaxis, I.D. Stamou, N. Tetradis and A. Tsigkas-Kouvelis, *Spectrum oscillations from features in the potential of single-field inflation*, *Phys. Rev. D* **104** (2021) 103510 [[2106.02467](#)].
- [59] K. Inomata, E. McDonough and W. Hu, *Amplification of primordial perturbations from the rise or fall of the inflaton*, *JCAP* **02** (2022) 031 [[2110.14641](#)].
- [60] Y.-F. Cai, X.-H. Ma, M. Sasaki, D.-G. Wang and Z. Zhou, *One small step for an inflaton, one giant leap for inflation: A novel non-Gaussian tail and primordial black holes*, *Phys. Lett. B* **834** (2022) 137461 [[2112.13836](#)].
- [61] R. Kawaguchi, T. Fujita and M. Sasaki, *Highly asymmetric probability distribution from a finite-width upward step during inflation*, *JCAP* **11** (2023) 021 [[2305.18140](#)].
- [62] X. Wang, X.-H. Ma and M. Sasaki, *A complete analysis of inflation with piecewise quadratic potential*, [2412.16463](#).
- [63] Y. Cai, M. Zhu and Y.-S. Piao, *Primordial black holes from null energy condition violation during inflation*, [2305.10933](#).
- [64] C. Pattison, V. Vennin, H. Assadullahi and D. Wands, *Quantum diffusion during inflation and primordial black holes*, *JCAP* **10** (2017) 046 [[1707.00537](#)].
- [65] C. Animali and V. Vennin, *Clustering of primordial black holes from quantum diffusion during inflation*, *JCAP* **08** (2024) 026 [[2402.08642](#)].
- [66] V. Vennin and D. Wands, *Quantum diffusion and large primordial perturbations from inflation*, [2402.12672](#).
- [67] C. Germani and R.K. Sheth, *Nonlinear statistics of primordial black holes from Gaussian curvature perturbations*, *Phys. Rev. D* **101** (2020) 063520 [[1912.07072](#)].
- [68] M. Shibata and M. Sasaki, *Black hole formation in the Friedmann universe: Formulation and computation in numerical relativity*, *Phys. Rev. D* **60** (1999) 084002 [[gr-qc/9905064](#)].
- [69] S. Young, C.T. Byrnes and M. Sasaki, *Calculating the mass fraction of primordial black holes*, *JCAP* **07** (2014) 045 [[1405.7023](#)].
- [70] V. De Luca and A. Riotto, *A note on the abundance of primordial black holes: Use and misuse of the metric curvature perturbation*, *Phys. Lett. B* **828** (2022) 137035 [[2201.09008](#)].
- [71] S. Raatikainen, S. Rasanen and E. Tomberg, *Primordial black hole compaction function from stochastic fluctuations in ultra-slow-roll inflation*, [2312.12911](#).
- [72] A. Escrivà, C. Germani and R.K. Sheth, *Universal threshold for primordial black hole formation*, *Phys. Rev. D* **101** (2020) 044022 [[1907.13311](#)].
- [73] J.M. Bardeen, J.R. Bond, N. Kaiser and A.S. Szalay, *The Statistics of Peaks of Gaussian Random Fields*, *Astrophys. J.* **304** (1986) 15.
- [74] C.-M. Yoo, T. Harada, J. Garriga and K. Kohri, *Primordial black hole abundance from random Gaussian curvature perturbations and a local density threshold*, *PTEP* **2018** (2018) 123E01 [[1805.03946](#)].
- [75] C.-M. Yoo, J.-O. Gong and S. Yokoyama, *Abundance of primordial black holes with local non-Gaussianity in peak theory*, *JCAP* **09** (2019) 033 [[1906.06790](#)].
- [76] C.-M. Yoo, T. Harada, S. Hirano and K. Kohri, *Abundance of Primordial Black Holes in Peak Theory for an Arbitrary Power Spectrum*, *PTEP* **2021** (2021) 013E02 [[2008.02425](#)].
- [77] N. Kitajima, Y. Tada, S. Yokoyama and C.-M. Yoo, *Primordial black holes in peak theory with a non-Gaussian tail*, *JCAP* **10** (2021) 053 [[2109.00791](#)].

- [78] V. Atal, J. Garriga and A. Marcos-Caballero, *Primordial black hole formation with non-Gaussian curvature perturbations*, *JCAP* **09** (2019) 073 [[1905.13202](#)].
- [79] V. Atal, J. Cid, A. Escrivà and J. Garriga, *PBH in single field inflation: the effect of shape dispersion and non-Gaussianities*, *JCAP* **05** (2020) 022 [[1908.11357](#)].
- [80] A. Escrivà, C. Germani and R.K. Sheth, *Analytical thresholds for black hole formation in general cosmological backgrounds*, *JCAP* **01** (2021) 030 [[2007.05564](#)].
- [81] M.W. Choptuik, *Universality and scaling in gravitational collapse of a massless scalar field*, *Phys. Rev. Lett.* **70** (1993) 9.
- [82] C.R. Evans and J.S. Coleman, *Observation of critical phenomena and selfsimilarity in the gravitational collapse of radiation fluid*, *Phys. Rev. Lett.* **72** (1994) 1782 [[gr-qc/9402041](#)].
- [83] T. Koike, T. Hara and S. Adachi, *Critical behavior in gravitational collapse of radiation fluid: A Renormalization group (linear perturbation) analysis*, *Phys. Rev. Lett.* **74** (1995) 5170 [[gr-qc/9503007](#)].
- [84] J.C. Niemeyer and K. Jedamzik, *Near-critical gravitational collapse and the initial mass function of primordial black holes*, *Phys. Rev. Lett.* **80** (1998) 5481 [[astro-ph/9709072](#)].
- [85] A.M. Green and A.R. Liddle, *Critical collapse and the primordial black hole initial mass function*, *Phys. Rev. D* **60** (1999) 063509 [[astro-ph/9901268](#)].
- [86] I. Musco, J.C. Miller and A.G. Polnarev, *Primordial black hole formation in the radiative era: Investigation of the critical nature of the collapse*, *Class. Quant. Grav.* **26** (2009) 235001 [[0811.1452](#)].
- [87] I. Musco and J.C. Miller, *Primordial black hole formation in the early universe: critical behaviour and self-similarity*, *Class. Quant. Grav.* **30** (2013) 145009 [[1201.2379](#)].
- [88] A. Escrivà, *Simulation of primordial black hole formation using pseudo-spectral methods*, *Phys. Dark Univ.* **27** (2020) 100466 [[1907.13065](#)].
- [89] K. Inomata and T. Nakama, *Gravitational waves induced by scalar perturbations as probes of the small-scale primordial spectrum*, *Phys. Rev. D* **99** (2019) 043511 [[1812.00674](#)].
- [90] K. Saikawa and S. Shirai, *Primordial gravitational waves, precisely: The role of thermodynamics in the Standard Model*, *JCAP* **05** (2018) 035 [[1803.01038](#)].
- [91] A. Escrivà, V. Atal and J. Garriga, *Formation of trapped vacuum bubbles during inflation, and consequences for PBH scenarios*, *JCAP* **10** (2023) 035 [[2306.09990](#)].
- [92] M. Shimada, A. Escrivà, D. Saito, K. Uehara and C.-M. Yoo, *Primordial Black Hole Formation from Type II Fluctuations with Primordial Non-Gaussianity*, [2411.07648](#).
- [93] D. Baumann, P.J. Steinhardt, K. Takahashi and K. Ichiki, *Gravitational Wave Spectrum Induced by Primordial Scalar Perturbations*, *Phys. Rev. D* **76** (2007) 084019 [[hep-th/0703290](#)].
- [94] K. Kohri and T. Terada, *Semianalytic calculation of gravitational wave spectrum nonlinearly induced from primordial curvature perturbations*, *Phys. Rev. D* **97** (2018) 123532 [[1804.08577](#)].
- [95] J.R. Espinosa, D. Racco and A. Riotto, *A Cosmological Signature of the SM Higgs Instability: Gravitational Waves*, *JCAP* **09** (2018) 012 [[1804.07732](#)].
- [96] J.-P. Li, S. Wang, Z.-C. Zhao and K. Kohri, *Primordial non-Gaussianity  $f_{NL}$  and anisotropies in scalar-induced gravitational waves*, *JCAP* **10** (2023) 056 [[2305.19950](#)].
- [97] P. Adshead, K.D. Lozanov and Z.J. Weiner, *Non-Gaussianity and the induced gravitational wave background*, *JCAP* **10** (2021) 080 [[2105.01659](#)].
- [98] K.T. Abe, R. Inui, Y. Tada and S. Yokoyama, *Primordial black holes and gravitational waves induced by exponential-tailed perturbations*, *JCAP* **05** (2023) 044 [[2209.13891](#)].

- [99] R.-g. Cai, S. Pi and M. Sasaki, *Gravitational Waves Induced by non-Gaussian Scalar Perturbations*, *Phys. Rev. Lett.* **122** (2019) 201101 [[1810.11000](#)].